The Roles of Four Conserved Basic Amino Acids in a Ferredoxin-Dependent Cyanobacterial Nitrate Reductase.

ARTICLE *in* BIOCHEMISTRY · MAY 2013

Impact Factor: 3.02 · DOI: 10.1021/bi400354n · Source: PubMed

14 AUTHORS, INCLUDING:

Anurag P Srivastava
Texas Tech University
4 PUBLICATIONS **7** CITATIONS
SEE PROFILE

Masakazu Hirasawa
Texas Tech University
89 PUBLICATIONS **2,836** CITATIONS
SEE PROFILE

Enrique Flores
Spanish National Research Council
163 PUBLICATIONS **6,249** CITATIONS
SEE PROFILE

David B Knaff
Texas Tech University
220 PUBLICATIONS **5,767** CITATIONS
SEE PROFILE

Published in final edited form as:
Biochemistry. 2013 June 25; 52(25): 4343–4353. doi:10.1021/bi400354n.

The Roles of Four Conserved Basic Amino Acids in a Ferredoxin-Dependent Cyanobacterial Nitrate Reductase

Anurag P. Srivastava[1,‡], **Masakazu Hirasawa**[1,‡], **Megha Bhalla**[1,†], **Jung-Sung Chung**[1,¶], **James P. Allen**[2], **Michael K. Johnson**[3], **Jatindra N. Tripathy**[4], **Luis M. Rubio**[5], **Brian Vaccaro**[3], **Sowmya Subramanian**[3,#], **Enrique Flores**[6], **Masoud Zabet-Moghaddam**[4], **Kyle Stitle**[1], and **David B. Knaff**[1,4,*]

[1]Department of Chemistry and Biochemistry, Texas Tech University, Lubbock, Texas 79409-1061, U.S.A

[2]Department of Chemistry and Biochemistry, Arizona State University, Tempe, Arizona 85287-1604, U.S.A

[3]Department of Chemistry and Center for Metalloenzyme Studies, University of Georgia, Athens, Georgia 30602-2556, U.S.A

[4]Center for Biotechnology and Genomics, Texas Tech University, Lubbock, Texas 79409-3132, U.S.A

[5]Centro de Biotecnología y Genómica de Plantas (UPM-INIA), Universidad Politécnica de Madrid, Campus de Montegancedo, Pozuelo de Alarcón, 28223 Madrid, Spain

[6]Instituto de Bioquímica Vegetal y Fotosíntesis, Consejo Superior de Investigaciones Científicas and Universidad de Sevilla, E-41092 Seville, Spain

Abstract

The roles of four conserved basic amino acids in the reaction catalyzed by the ferredoxin-dependent nitrate reductase from the cyanobacterium *Synechococcus* sp. PCC 7942 have been investigated using site-directed mutagenesis in combination with measurements of steady-state kinetics, substrate-binding affinities and spectroscopic properties of the enzyme's two prosthetic groups. Replacement of either Lys58 or Arg70 by glutamine leads to a complete loss of activity, with both the physiological electron donor, reduced ferredoxin and with a non-physiological electron donor, reduced methyl viologen. More conservative, charge-maintaining K58R and R70K variants were also completely inactive. Replacement of Lys130 by glutamine produced a variant that retained 26% of the wild-type activity with methyl viologen as the electron donor and 22% of the wild-type activity with ferredoxin as the electron donor, while replacement by arginine produces a variant that retains a significantly higher percentage of the wild-type activity with both electron donors. In contrast, replacement of Arg146 by glutamine had minimal effect on the activity of the enzyme. These results, along with substrate-binding and spectroscopic measurements, are discussed in terms of an *in silico* structural model for the enzyme.

The pathway for nitrate assimilation in cyanobacteria (1,2) involves an initial two-electron reduction of nitrate to nitrite catalyzed by nitrate reductase, followed by the six-electron

*To whom correspondence should be addressed: Telephone, 806 742 0288; FAX, 806 742 1289; david.knaff@ttu.edu.
‡These two authors contributed equally to the work.
†Current Address Biological Dynamics, Inc., San Diego, CA 92121, U.S.A.
¶Current Address: Department of Agronomy, Institute of Agricultural and Life Sciences, Gyeongsang National University, Jinju 660-701, Republic of Korea.
#Current Address: New Mexico Consortium, 4200 W Jemez Rd, Ste 301, Los Alamos, NM 87544

reduction of nitrite to ammonia and the subsequent incorporation of this ammonia to form glutamine (glutamine formation involves ATP but does not involve any redox chemistry). Glutamine then reacts with 2-oxoglutarate, in a two-electron reduction, to form two molecules of glutamate, in the final step of the reductive portion of the nitrate assimilation pathway (1,2). In cyanobacteria, uniquely, all three of the reductant-requiring steps utilize reduced ferredoxin (Fd) as the specific physiological electron donor (1,2). In contrast, in oxygenic photosynthetic eukaryotes, while ferredoxin is the electron donor for both the reduction of nitrite to ammonia and of glutamine plus 2-oxoglutarate to glutamate, the reduction of nitrate to nitrite utilizes reduced pyridine nucleotide as the reductant (1,3).

Among the best characterized of the cyanobacterial ferredoxin-dependent nitrate reductases is that from *Synechococcus* sp. PCC 7942 (NarB). This 78 kDa, soluble, monomeric enzyme contains a single [4Fe-4S] cluster and a single Mo *bis*-molybdopterin guanine dinucleotide (MoMGD) center as its only prosthetic groups (4). The redox chemistry of these two prosthetic groups has been investigated, using a combination of electron paramagnetic resonance (EPR) spectroscopy and potentiometry (5). The oxidized $[4Fe\text{-}4S]^{2+}$ form of the iron-sulfur cluster is EPR silent, while one-electron reduction ($E_m = -190$ mV) produces a signal at 10 K characteristic of a $[4Fe\text{-}4S]^{1+}$ cluster. Redox titrations, combined with EPR spectra obtained at 60 K, indicated a Mo(VI) to Mo(V) transition ($E_m = -150$ mV), with the Mo (V) species displaying a “high g” EPR signal ($g_{av} = 1.9897$). Protein film voltammetry measurements suggested that the nitrate binds to the enzyme during the catalytic cycle when the enzyme is in a two-electron reduced state containing the $[4Fe\text{-}4S]^{1+}$ form of the cluster and MDG in the Mo(V) oxidation state (5).

The *Synechococcus* sp. PCC 7942 nitrate reductase has been shown to form a high-affinity, 1:1 complex with ferredoxin at low ionic strength (6). The observation that the complex dissociates at high ionic strength (6) suggested that electrostatic forces might play a role in stabilizing the complex. Experiments with charge-replacement variants of ferredoxin were consistent with the hypothesis that negatively-charged amino acid side chains on ferredoxin contributed to its interaction with *Synechococcus* sp. PCC 7942 nitrate reductase (6). The observation that chemical modification of nitrate reductase with either phenylglyoxal or N-acetylsuccinimide, reagents known to eliminate the positive charges on the side chains of arginine or lysine residues, respectively, interfered with complex formation between the enzyme and ferredoxin (6) was also consistent with the hypothesis that electrostatic interactions played a role in stabilizing this complex.

To further explore possible role(s) of basic amino acids in nitrate reductase, we have used site-directed mutagenesis to examine the requirement for the presence of two conserved lysine residues and two conserved arginine residues in *Synechococcus* sp. PCC 7942 nitrate reductase. The fact that these four residues are conserved in all known cyanobacterial nitrate reductases (there are currently at least 126 sequenced cyanobacterial genomes – Ref. 7) identified them as appropriate targets for an initial mutagenesis study. Figure 1 shows an alignment, for a portion of the amino acid sequences of ferredoxin-dependent nitrate reductases, from six representative cyanobacterial species, showing the sequence positions of the four residues in question. Although no three-dimensional structures are available for any ferredoxin-dependent cyanobacterial nitrate reductases, the fact that structures for related enzymes are available (8–12) has enabled us to model a possible structure for the *Synechococcus* sp. PCC 7942 nitrate reductase. Figure 2 shows this *in silico* model and highlights the predicted positions of these four residues with respect to the [4Fe-4S] cluster and MGD prosthetic groups of the enzyme. Table 1 summarizes the shortest distances, in the *in silico* model, from each of the four conserved residues studied to the two prosthetic groups of the enzyme. Below, we report the effect of eliminating these four positive charges

by replacing each of the residues with the uncharged polar amino acid glutamine, on the kinetic, spectroscopic and substrate-binding properties of the enzyme.

Materials and Methods

A plasmid, designated pCSLM85 and previously described in detail (4), was used to direct the expression of wild-type *Synechococcus* sp. PCC 7942. The plasmid contains a modified form of the *narB* gene, encoding nitrate reductase, in which the codons for the first 14 amino acids have been deleted and six histidine codons were fused at the 3′ terminus of the gene (This truncation at the N-terminus reflects the likely status of the mature form of the enzyme *in vivo* – Ref. 4. The amino acid numbering system used for *Synechococcus* sp. PCC 7942 nitrate reductase in this manuscript denotes the N-terminal methionine in the truncated, expressed protein as amino acid number 1.). Cells of *Escherichia coli* strain DH5a (Stratagene) were transformed with pCSLM85 and grown aerobically overnight, with shaking, at 37 °C in Luria-Bertani (LB) medium containing 100 μg/ml ampicillin. An aliquot of this culture was used to inoculate LB medium containing 100 μg/ml ampicillin and the culture was allowed to grow aerobically at 37 °C, with shaking at 225 rpm. When the optical density of the culture at 600 nm was between 0.6 and 0.8, isopropyl-β-D-thiogalactopyranoside (IPTG), at a final concentration of 1 mM, was added to the culture. Sodium molybdate (final concentration = 100 μM) was also added in the culture at this time. The cells were then grown for 5–6 hours at 30 °C, at a lower shaking speed (175–200 rpm) and harvested by centrifugation at 8,000 × g for 8 minutes at 4 °C. The cell pellet was resuspended in buffer A containing 25 mM HEPES (pH 8.0), 50 mM NaCl, 1 mM imidazole, 100 μM sodium molybdate and 10% glycerol. A cocktail of protease inhibitors containing phenylmethylsulfonyl fluoride (PMSF), aminocaproic acid and benzamidine, each at 1 mM final concentration, was also included. Cells were lysed by two passages through a French Press at 12,000 p.s.i. Cell debris was removed by centrifugation at 40,000 × g for 30 min at 4 °C (All subsequent purification steps were also carried out at 4 °C.). The resulting particulate-free supernatant was loaded onto a 25-ml TALON column containing resin charged with cobalt (Clontech) for purification of the nitrate reductase by immobilized metal affinity chromatography. The column was washed thoroughly with buffer A containing 20 mM imidazole and the nitrate reductase was eluted with buffer A containing 200 mM imidazole. Imidazole was removed by 5 cycles, each of which involved dilution with imidazole-free buffer followed by concentration using a Centricon concentrator (Millipore Corp.) with a 50 kDa cutoff membrane (this same concentrator was used for all subsequent concentration steps). The concentrated protein solution was then loaded on a DEAE-cellulose (DE-52, Whatman) column equilibrated with buffer B containing 25 mM HEPES (pH 8.0), 50 mM NaCl and 100 μM sodium molybdate. The column was washed with buffer B containing 100 mM NaCl and protein was eluted with buffer B containing 200 mM NaCl. The eluted protein was concentrated, loaded onto a 1.5 × 100 cm Ultrogel AcA 44 gel filtration column (BioSpera) and eluted with buffer containing 25 mM HEPES (pH 8.0), 200 mM NaCl and 100 μM sodium molybdate.

Single amino acid replacement variants of nitrate reductase were prepared by site-directed mutagenesis of the *narB* gene using the QuickChange™ (QC) site-directed mutagenesis kit (Stratagene) and the protocol recommended by the vendor. Site-specific replacement of Lys58 and Lys130 and of Arg70 and Arg146 were accomplished using a polymerase chain reaction (PCR) technique with primers (See Table 2) purchased from Integrated DNA Technologies. PCR amplification with these primers was catalyzed by the high fidelity DNA polymerase supplied with the kit. PCR amplifications were carried out in 50 Xl solutions containing 50 ng of template DNA, 125 ng each of both forward and reverse primers, 0.2 mM deoxyribonucleotide triphosphates and 2.5 units of *pfuTurbo*® DNA polymerase. After an initial DNA template strand separation at 95 °C for 3 minutes, 16 PCR cycles were

carried out, each with denaturation at 95 °C for 1 minute, annealing at 55 °C for 1 minute and extension for 8 minutes at 68 °C. The PCR product was then incubated at 37 °C for 1 hour with 10 units of the *DpnI* provided as part of the mutagenesis kit to digest the template DNA. After *DpnI* digestion, 1–2 Xl of digestion product was used to transform cells of the DH5a strain of *E. coli*, using a 45-second heat shock at 42 °C followed by incubation on ice for 3 minutes. After transformation, cells were incubated for one hour at 37 °C with shaking and transformed cells were selected using LB agar plates containing 100 μg/ml of ampicillin. A transformed single colony was picked and grown overnight in 5 ml of ampicillin-containing LB medium at 37 °C. Plasmids were isolated from these cultures using a plasmid isolation mini-kit (QIAGEN). The nitrate-reductase coding domains of all the mutated plasmids were sequenced, using specific sequencing primers, in the Texas Tech University Center for Biotechnology and Genomics Core Facility to confirm the mutations. The same expression and purification procedure was followed for all of the single amino acid replacement nitrate reductase variants produced by mutagenesis. All enzyme samples were stored at −80 °C prior to use.

Wild-type *Synechocystis* sp. PCC 6803 ferredoxin was expressed in *E. coli* and purified as described previously (13) and stored at −80 °C prior to use. SDS-PAGE and MALDI-TOF mass spectrometry analyses indicated that the protein was at least 95% pure. Ferredoxin from *Synechococcus* sp. PCC 7002 was expressed in *E. coli* and prepared using the same protocol used for the preparation of the *Synechocystis* sp. PCC 6803 ferredoxin. Spinach ferredoxin was prepared from spinach leaf as described previously (14).

UV/visible absorbance spectra and difference absorbance spectra were obtained using a Shimadzu Model UV-2401PC spectrophotometer, at a spectral resolution of 0.5 nm. Circular dichroism (CD) spectra, at a spectral resolution of 1.0 nm, were obtained using an OLIS model DSM-10 UV-Vis CD spectrophotometer. X-band (~9.6 GHz) electron paramagnetic resonance (EPR) spectra were recorded in the Department of Chemistry at the University of Georgia on a Bruker ESP-300E EPR spectrometer equipped with an ER-4116 dual-mode cavity and an Oxford Instruments ESR-9 flow cryostat. Spin quantifications were carried out under non-power saturation conditions using a 1 mM CuEDTA standard as described by Aasa and Vänngård (15).

Ferredoxin concentrations were measured from the absorbance at 420 nm, using an extinction coefficient of 9.7 $mM^{-1}cm^{-1}$ (14). Nitrate reductase concentrations were measured according to the method of Bradford (16), using bovine serum albumin as a standard. Acid-labile sulfide contents were measured as described by Siegel *et al.* (17). The Fe and Mo contents were determined using inductively coupled plasma (ICP) mass spectrometry in the Department of Chemistry and Biochemistry at Arizona State University. A Thermo Scientific X-series spectrometer, with Ge as an internal standard, was used to make all of the measurements. The metals were released from the protein samples by adding 2% nitric acid and heating for 15 minutes at 45 °C. After heating, the denatured protein was removed by centrifugation and the supernatants were diluted in water, with the final protein concentration always adjusted so that, if the sample had a fully-occupied iron-sulfur cluster site, the measured iron concentration would be 30 parts per billion. Fe was measured using a 7% hydrogen/93% helium collision gas to reduce the formation of argon oxide at mass 56. For both Fe and Mo, all measurements were run in triplicate, along with triplicate determinations of protein-free blank controls. The values reported represent the averages of the three determinations, after subtraction of the average values for the blank controls.

Matrix-Assisted Laser Desorption Ionization-Time of Flight (MALDI-TOF) mass spectrometry, utilizing an Applied Biosystems 4800 Plus MALDI TOF/TOF spectrometer containing a 355-nm Nd-YAG laser operating in a positive ion mode, was used to determine

the molecular masses of wild-type nitrate reductase and of ferredoxin. One XL of concentrated protein solution was mixed with 5 XL of a 30 mM sinapinic acid solution (as matrix) and 0.5 XL of this mixture was spotted onto the MALDI plate. Bovine serum albumin and lysozyme were used as molecular mass standards for calibration of the instrument.

Nitrate reductase activities, with either reduced methyl viologen (MV) or reduced ferredoxin as the electron donor, were measured as carried out previously (6). All plots of nitrate reductase activity as a function of ferredoxin concentration at saturating nitrate concentration and as a function of nitrate concentration at saturating ferredoxin concentration gave excellent fits to the Michaelis-Menten Equation. Kinetic parameters were calculated by fitting the data (i.e., initial velocity *vs.* substrate concentration) to the Michaelis-Menten equation using GraphPad Prism 6 software. Complex formation between ferredoxin and nitrate reductase was measured using the previously described spectral perturbation method (6), except for the choice of the wavelength pairs used to monitor complex formation. Complex formation for wild-type nitrate reductase was monitored at 420 nm *minus* 600 nm. Variations were observed in the maxima of the difference spectrum, depending on the nitrate reductase variant, and so to maximize the magnitude of the absorbance changes used for the K_d calculations, the following wavelength pairs were used to monitor ferredoxin binding by the variants: K58Q, 370 nm *minus* 430 nm; K58R, 410 nm *minus* 470 nm; R70Q, 365 nm *minus* 410 nm; R70K, 320 nm *minus* 470 nm; K130Q, 390 nm *minus* 450 nm, K130R, 300 nm *minus* 370 nm; and R146Q, 420 nm *minus* 460 nm. Complex formation between nitrate reductase and nitrate was also measured using this spectral perturbation method and, with the absorbance change observed at saturating nitrate taken to represent 100% complex formation. As was the case for complex formation with ferredoxin, different wavelength pairs were used for the different variants to maximize the signal:noise ratio of the absorbance changes used to monitor complex formation. The wavelength pairs used were: Wild-type, 400 nm *minus* 470 nm; K58Q, 500 nm *minus* 600 nm; K58R, 300 nm *minus* 370 nm; R70Q, 365 nm *minus* 410 nm; R70K, 290 nm *minus* 360 nm; K130Q, 320 nm *minus* 390 nm; K130R, 480 nm *minus* 640 nm and R146Q, 420 nm *minus* 500 nm. Dissociation constant (K_d) values were calculated by fitting the data (i.e., the magnitude of the spectral perturbation change *vs.* ligand concentration) to the equation for a single binding isotherm GraphPad Prism 6 software.

An *in silico* model of a likely three dimensional structure of wild-type *Synechococcus* sp. PCC 7942 nitrate reductase was calculated, using the structure (PDB entry 2NAP) of the dissimilatory nitrate reductase from *Desulfovibrio desulfuricans* (11) as the starting model. The structural model for the *Synechococcus* sp. PCC 7942 enzyme contains amino acid residues 36 to 755 (using the residue numbering system described above and in the first entry in Figure 1), as well as the cofactors. The model was modified assuming that *Synechococcus* sp. PCC 7942 and *D. desulfuricans* nitrate reductases have similar folds. The two sequences were aligned using CLUSTAL W and the amino acids of the structural model were systematically changed according to the CLUSTAL alignment, with minor modifications. Gaps were inserted using COOT (18). For each substitution the position of the altered side chain was chosen based upon the preferred rotomer (i.e., one that did not cause any steric clashes). Local minimization was performed as needed. The resulting model runs from amino acid 1 to 709, but excludes the nonconserved regions (i.e., 22–40, 257–259, 548–552, 673–679, 710–715). After all of the substitutions, the entire model was energy minimized using CHIMERA (19). The distances reported between cofactors and amino acid residues are calculated between the ends of the amino acid side chain and the closest points of the cofactor.

Results

Before ascertaining the purity of the nitrate reductase samples used in this study, the purity of the ferredoxins used was checked using both SDS-PAGE and UV/visible absorbance spectra. Both methods, indicated purities of at least 95%. As a further test of ferredoxin purity, mass spectrometry was also used and during the course of the mass spectrometry measurements, it became apparent that the results also provided information about the identity of the N-terminal amino acid of two cyanobacterial ferredoxins used in this investigation. Structures previously determined for *Synechocystis* sp. PCC 6803 ferredoxin, both by X-ray crystallography (20,21 and PDB entries 1OFF and 2PVG) and NMR spectroscopy (22,23 and PDB entries1DOX and 2KAJ), for recombinant protein that had been expressed in *E. coli*, indicated that the protein's initial methionine is post-translationally cleaved during expression and that the N-terminal amino acid of the expressed protein is the alanine that was originally in the second position in the sequence encoded by the gene. MALDI-TOF analysis of the recombinant *Synechocystis* sp. PCC 6803 ferredoxin used in the studies described below indicated that its molecular mass is 10,237 Da. This value is in good agreement, within the experimental uncertainty in the measurement, with the 10,232 Da mass calculated for a 96 amino long protein beginning with alanine, and is in much better agreement than with the 10,347 Da value calculated for a 97 amino acid long protein that begins with methionine. Analysis of a tryptic digest of *Synechocystis* Fd showed no evidence for the presence of peak at m/z = 799 that would correspond to the theoretical mass for the N-terminal tryptic peptide MASYTVK that would be expected if the N-terminal amino acid were methionine. Instead, a peak at m/z = 669 was detected, in excellent agreement with the theoretical mass of the peptide ASYTVK, providing strong additional confirmation that the initial methionine of *Synechocystis* sp. PCC 6803 ferredoxin used as an electron donor to nitrate reductase for the activity measurements described below is cleaved off during expression in *E. coli*. Similar mass spectrometry data for the ferredoxin from *Synechococcus sp*. PCC 7002, expressed in *E. coli*, indicated that it is also missing the initial methionine and that the N-terminal amino acid of the recombinant protein is alanine.

The yield of wild-type nitrate reductase was approximately 7.8 mg of purified protein per liter of *E. coli* culture and the yields for all but one of the variants used in this study ranged from 2.5 mg/L for K58Q to 9.3 mg/L for R146Q. However, for reasons that are not clear, a very much lower yield of 0.4 mg of purified protein per liter of *E. coli* culture was obtained for the K130Q variant. It is worth mentioning that the addition of 100 μM molybdate to the growth medium for the *E. coli* cells used to express recombinant nitrate reductase using the protocol currently being followed at Texas Tech University (see Materials and Methods) produced a significant increase in the average Mo content of the enzyme and eliminated the problem, occasionally encountered before the growth protocol was changed to include molybdate, of obtaining wild-type enzyme that typically contained only 0.3 to 0.5 mol Mo/mol enzyme. SDS-PAGE analysis, followed by staining with Coomassie Brilliant Blue, indicated that all of the enzyme samples used in this study were at least 90% pure and had an approximate molecular mass of 78 kDa. The specific activities of the wild-type enzyme, with either reduced ferredoxin or with reduced methyl viologen serving as the electron donor, are somewhat higher than those reported previously (4), i.e., 23% higher in the case of the MV-dependent activity and 29% higher in the case of the Fd-dependent activity. The ratio of MV-dependent activity to Fd-dependent activity displayed by wild-type enzyme, i.e., 31.5, is comparable to, but somewhat lower than, the value of 33.0 reported previously (4), as a result of the larger improvement in Fd-dependent activity relative to MV-dependent activity. MALDI-TOF mass spectrometry of the wild-type enzyme confirmed that the purity of the wild-type enzyme was > 90% and gave an estimated mass of 79,821 Da for the enzyme. This mass is higher than the 79,041 Da value calculated for the His-tagged apo-

enzyme from its known amino acid sequence and the 780 Da difference in mass may arise from partial retention of either the [4Fe-4S] cluster or the Mo-pterin center, or both. CD spectra, in the region from 200 nm to 300 nm of all of the variants used in this study were quite similar to that obtained for the wild-type enzyme, indicating that the mutational replacements introduced did not produce any major changes in the secondary structure of the enzyme. Even in the cases of variants, such as K58Q and K130Q that exhibited little or low activity, the observed differences in CD spectra, compared to that of wild-type nitrate reductase, were relatively small (Figure 3).

Table 3 summarizes the effects of replacing each of the four positively-charged amino acids under study with the polar, but uncharged, amino acid glutamine on the enzyme's kinetic parameters with both *Synechocystis* sp. PCC 6803 ferredoxin and with methyl viologen serving as the electron donor. It should be mentioned that essentially identical effects of these nitrate reductase mutational replacements were observed when *Synechocystis* sp. PCC 6803 ferredoxin was replaced either by ferredoxin isolated from spinach leaf or by recombinant ferredoxin from the cyanobacterium *Synechococcus sp*. PCC 7002 (data not shown). Replacing either Lys58 or Arg70 had the most dramatic effect on the enzymatic activity of the enzyme, completely abolishing activity with both the physiological electron donor, i.e., reduced ferredoxin, and a non-physiological, small molecule electron donor, reduced methyl viologen. More conservative replacements, in which a positively-charged lysine is replaced by a positively-charged arginine, or *vice versa*, produced the same total loss of activity effect as did the charge elimination replacement with glutamine at both position 58 and 70. Thus it appears, at least at these two positions, that a positive charge on a side chain by itself is not sufficient for activity, but rather that lysine is specifically required at position 58 and arginine is specifically required at position 70. The apparent absolute requirement for a lysine residue at this position in *Synechococcus* sp. PCC 7942 nitrate reductase is in contrast to observations reported for the equivalent lysine, Lys85, in the catalytic subunit of the periplasmic nitrate reductase of *Ralstonia eutropha* H16. Activity measurements made with crude periplasmic extracts of *R. eutropha* showed that a K85R variant retained 23% of the activity exhibited by the wild-type enzyme while a K85M variant was completely inactive (24).

Arg146 lies at the other extreme from Lys58 and Arg70 in so far as an essential role in nitrate reductase catalysis is concerned. Replacement by glutamine has only small effects on either activity (i.e., a 9% loss in MV-dependent activity and a 13% loss in Fd-dependent activity, compared to the wild-type values). The observation that replacing the positively-charged arginine by the uncharged amino acid glutamine at position 146 produced virtually no loss in activity, made it seem unnecessary to prepare a Arg/Lys replacement variant at this position as a control. Nitrate reductase Lys130 occupies an intermediate position on the scale of activity loss that results from its replacement. Its replacement by glutamine leads to major losses in both the MV-dependent and Fd-dependent activities. Unlike the case for replacement of Lys58 and Arg70, where the replacement variants are completely inactive, the K130Q variant retains 26 % of the MV-dependent activity and 22% of the Fd-dependent activity of the wild-type enzyme. The replacement of this lysine by arginine, conserving the positive charge on the side chain, produces a variant that retains considerably more activity than does the glutamine-replacement one, i.e., 55% of the MV-dependent activity and 65% of the Fd-dependent activity. The K_x for ferredoxin exhibited by the K130R variant, i.e., 40 μM, is also closer to the 38 μM value measured for the wild-type enzyme than the 106 μM value for the K130Q variant. Also (See Table 4 below), the sulfide, Fe and Mo contents of the K130R variant are somewhat higher than that of the K130Q variant, indicating that the more conservative replacement results in better retention of the [4Fe-4S] cluster and MDG prosthetic groups than is the case for the less conservative glutamine replacement. The effects of replacing conserved residues at positions 58, 70 and 130 on steady-state enzyme

activity parameters are much more apparent in the V_{max} values than in the smaller effects on K_M (See Table 3). It should also be mentioned that, replacements at positions 130 and 146 produced small, but statistically significant increases in the ratio of MV-dependent to Fd-dependent activities. The reasons for the greater effects on the ferredoxin-dependent activity are currently under investigation.

As it is to be expected that nitrate reductase catalytic activity depends on full occupancy of both the [4Fe-4S] cluster and MoMGD sites by these prosthetic groups, it was of interest to determine the levels of the prosthetic groups in the mutated variants in order to determine whether the loss of activity observed with the variants with replacements at positions 58, 70, and 130 resulted from a simple loss of MoMGD and/or [4Fe-4S] cluster. Table 4 shows that the sulfide content measured for the wild-type enzyme is 3.5 ± 0.2 mol of sulfide/mol of protein, i.e., only 12.5% less than the theoretical value of 4.0 expected from the known presence of a single [4Fe-4S] cluster per enzyme (4,5). As the sulfide assay depends on the complete trapping of the H_2S released from the protein upon acidification (17), slight underestimates of the sulfide contents of iron-sulfur cluster containing proteins are occasionally encountered. The 3.2 mol sulfide/mol enzyme content measured for the R146Q variant, although calculated to be only 91% of the value determined for the wild-type enzyme, may well be identical to that observed for wild-type enzyme, within the experimental uncertainties of the labile sulfide measurements. Given that the R146Q variant retains >90% of the activity observed for wild-type nitrate reductase (See Table 3), an essentially fully-occupied iron-sulfur cluster site is not surprising. In fact, none of the replacement variants examined show extremely large decreases in sulfide content when compared to the wild-type enzyme. For example, the K130Q variant that has lost 78% of its ferredoxin-dependent activity retains 89% of the sulfide found in wild-type enzyme and even the completely inactive K58Q, K58R, R70Q, and R70K variants have sulfide contents that are at least 77% of the wild-type enzyme value (the lowest sulfide content was observed for the K58Q variant), with a value equal to 86% of the value observed for the wild-type enzyme found in the case of the inactive R70K variant. Thus, there seems to be little or no correlation between the sulfide content of the variants studied and their activities. The case is somewhat different when iron contents are examined, with several variants (i.e., K58Q, K58R, and R70K), losing more than half of the iron found in the wild-type enzyme and with the R70Q variant losing almost this much. The loss is most extreme in the case of the K58Q variant, which has an iron content equal to only 20% that of the wild-type enzyme. Table 4 also summarizes the results of Mo analyses carried out on wild-type enzyme and on its variants. It is worth noting that, with the exception of the K58Q and R146Q variants, all of the variants show significantly lower Mo contents than the wild-type enzyme. Perhaps the most surprising result is that, in the case of two positions (i.e., at Lys58 and Arg70), conservative replacement of the positively-charged residue found in the native enzyme by another positively-charged residue (i.e., arginine for lysine or *vice versa*), produces a greater loss in Mo content than does replacement by glutamine. This is most striking at position 58, where the replacement of lysine by glutamine has no detectable effect on the Mo content of the enzyme, while replacement by arginine cause a 76% loss of Mo.

Figure 4 shows UV/visible region absorbance spectra for the wild-type enzyme and of its K58Q and K130Q variants over the spectral range from 300 nm to 600 nm (the spectra of the two variants were essentially identical to that of the wild-type enzyme in the spectral region from 250 nm to 300 nm – not shown). The significant decrease in absorbance in the visible region seen in the spectrum of the K58Q variant, when compared to the spectrum of the wild-type enzyme, is likely to arise mainly from the lower levels of [4Fe-4S] cluster in this variant.

The effect of the mutations on the properties of the MoMGD and [4Fe-4S] centers in the air-oxidized (as prepared) and dithionite-reduced forms of the enzyme were also assessed using X-band EPR spectroscopy (see Figure 5). EPR studies at 70 K and 2 mW microwave power were used to selectively investigate $S = 1/2$ Mo(V) species which, in contrast to $[3Fe\text{-}4S]^+$ and $[4Fe\text{-}4S]^+$ clusters, exhibit slow relaxation and consequently are readily observed without broadening at 70 K. As shown in Figure 5(A), aerobically purified samples of wild-type and the R146Q, K130Q, K130R, R70Q, and R70K variants all exhibit a "very high *g*" type, proton-split Mo(V) resonance ($g_{1,2,3} = 2.023, 1.998, 1.993$; $A_{1,2,3} = 6.8, 7.5, 6.8$ G) analogous to that observed in previous EPR studies of *Synechococcus* sp. PCC 7942 nitrate reductase (5). Spin quantitations coupled with the Mo quantitations shown in Table 4, indicate that EPR signals in these samples account for between 10–30% of the Mo content, in good accord with the10–20% of total Mo content previously reported for EPR spin quantitations of the wild-type enzyme (5). Overall the EPR results indicate that R146Q, K130Q, K130R, R70Q, and R70K mutations result in minimal perturbation of Mo cofactor. In contrast, the K58Q and K58R variants exhibit negligible Mo(V) EPR resonances. For the K58R variant, this can in part be rationalized by the low Mo content (~0.19 Mo/NarB). However, the high Mo content for the K58Q variant (~0.80 Mo/NarB), suggests that this mutation has a major effect on the redox properties of the Mo center, due to its close proximity to the Mo cofactor (see Figure 2).

EPR studies of the aerobically purified samples at 10 K and 1 mW reveal fast relaxing resonances $S = 1/2$ with a $g_{//} \sim 2.02$ and $g_{\perp} \sim 2.00$ (see Figure 5) that are only clearly visible below 30 K and are characteristic of a $S = 1/2$ $[3Fe\text{-}4S]^+$ cluster (25). For wild-type and the R146Q, K130Q, K130R, R70Q, and R70K variants, the $[3Fe\text{-}4S]^+$ cluster resonance is overlapped with a partially power saturated and broadened Mo(V) resonance and spin quantitations indicate that $[3Fe\text{-}4S]^+$ cluster concentrations account for < 10% of the Fe content. Based on the EPR studies of the dithionite reduced samples, these trace amounts of $[3Fe\text{-}4S]^+$ clusters are attributed to partial oxidative degradation of the indigenous $[4Fe\text{-}4S]^{2+,+}$ clusters during aerobic purification. This type of oxygen-induced cluster transformation is commonly observed for exposed [4Fe-4S] clusters, and is particularly prevalent in [4Fe-4S] clusters with one non-cysteinyl ligand (24). In contrast, spin quantitations of the intense $[3Fe\text{-}4S]^+$ cluster resonances observed for the K58Q and K58R variants account of all of the Fe content, within experimental error, indicating that these mutations make the $[4Fe\text{-}4S]^{2+,+}$ clusters much more sensitive to aerial oxidative degradation via a $[3Fe\text{-}4S]^+$ cluster intermediate.

EPR studies of the dithionite-reduced samples at 20 K and 1 mW microwave power facilitate assessment of effect of the mutations on the $[4Fe\text{-}4S]^+$ clusters. In accord with previous EPR studies (5), the dithionite-reduced wild-type enzyme exhibits a fast-relaxing, rhombic resonance ($g_{1,2,3} = 2.06$ 1.95 and 1.91) indicative of a $S = 1/2$ $[4Fe\text{-}4S]^+$ cluster. Since an identical resonance is observed for the R146Q, K130Q, K130R, R70Q, and R70K variants, EPR studies indicate that properties of $[4Fe\text{-}4S]^+$ cluster are unperturbed by these mutations. Moreover spin quantitations indicate that the $[4Fe\text{-}4S]^+$ resonances account for 80–100% of Fe content of these samples, see Table 4. In contrast, negligible $[4Fe\text{-}4S]^+$ resonances are observed for the K58Q and K58R variants indicating that minimal Fe^{2+}-induced conversion from the reduced $S = 2$ $[3Fe\text{-}4S]^0$ clusters to the $S = 1/2$ $[4Fe\text{-}4S]^+$ cluster occurs on dithionite reduction. This type of reductive cluster conversion occurs readily of many $[3Fe\text{-}4S]^+$ clusters generated by aerial oxidative damage of $[4Fe\text{-}4S]^{2+}$ clusters (25).

In addition to the fast relaxing resonance from the $S = 1/2$ $[4Fe\text{-}4S]^+$ cluster, a slow relaxing rhombic resonance, $g_{1,2,3} = 2.017, 1.988, 1.962$, is also observed in the 20-K EPR spectra of the WT and the R146Q, K130Q, K130R, R70Q, and R70K variants, but not in the K58Q

and K58R variants. This resonance is the sole resonance observed for the WT and the R146Q, K130Q, K130R, R70Q, and R70K variants at 70 K (data not shown) and accounts for between 3–10% of the total Mo concentration. Analogous Mo(V) resonances with negligible proton hyperfine and low spin quantitations have been observed for dithionite-reduced forms of other bacterial assimilatory nitrate reductases (26), and have been termed low-potential Mo(V) species. However, thus far we have been unable to observe the high-g Mo(V) signal in dithionite-reduced samples of *Synechococcus* sp. PCC 7942 nitrate reductase, as previously reported by Jepson et al (5). The origin of this discrepancy has yet to be resolved. Nevertheless, the agreement between the Mo(V) EPR signals seen in this work with other active forms of bacterial assimilatory nitrate reductases provides support for the observation that the Mo cofactor remains essentially intact in all mutants except K58Q and K58R.

The picture that emerges from the EPR results is that perturbation of the properties of the MoMGD cofactor or the [4Fe-4S] center in NarB are likely to be responsible for the complete loss of activity observed for the K58Q and K58R variants, but cannot be invoked to explain the complete loss of activity associated with the R70Q and R70K mutations.

In addition to the possibility that changes in prosthetic group content and/or properties could affect the activity of replacement variants, loss of activity could also arise from a decrease in substrate-binding affinities. To address this possibility, K_d values were measured for the electron-donating substrate, ferredoxin, and for the electron-accepting substrate, nitrate, using a spectral perturbation procedure developed previously for the wild-type, oxidized enzyme (6). It should be kept in mind that, in so far as ferredoxin is concerned, the actual substrate for nitrate reductase is reduced ferredoxin, while the K_d values shown in Table 4 were measured for oxidized ferredoxin. However, because reduced ferredoxin is so readily oxidized by even trace amounts of oxygen, studying binding of reduced ferredoxin to nitrate reductase requires essentially totally anaerobic conditions. Furthermore, because it would be extremely difficult to study the binding of reduced ferredoxin independently of subsequent electron transfer from ferredoxin to the enzyme, the data displayed in Table 4 were obtained with both proteins in their oxidized states. X-ray structures for the [2Fe-2S] ferredoxin from the cyanobacterium *Anabaena* sp. PCC 7119, a ferredoxin with very high sequence identity to the *Synechocystis* sp. PCC 6803 ferredoxin used in this study, indicate that the overall structures of the oxidized and reduced forms of the protein are quite similar (27). Thus, although some relatively small conformational changes in the immediate vicinity of the [2Fe-2S] cluster do occur on reduction (27), it seems likely that no great error will result from using K_d values for oxidized ferredoxin in assessing the affinity of the enzyme for reduced ferredoxin. Table 4 shows that, with the exception of the quite substantial ca. 11-fold increase in the K_d observed for the K58Q variant, replacement of the other three conserved basic amino acids by glutamine did not significantly decrease the affinity of the enzyme for oxidized ferredoxin and in a few cases (e.g., R70Q, R70K, and R146Q) actually produced a small increase in affinity. As perhaps might have been expected, in contrast to the 11-fold decrease in affinity for ferredoxin observed with the K58Q variant, the more conservative replacement of Lys58 by arginine produced a variant with wild-type affinity for ferredoxin (Table 4).

Table 4 also summarizes the data for nitrate binding by the wild-type enzyme and its variants. With the exception of the 8-fold increase in the K_d for nitrate binding observed for the inactive K58Q variant and the almost 20-fold increase observed with the very much inhibited K130Q variant, mutagenic replacement had relatively little effect on the affinity of the enzyme for nitrate. Somewhat surprisingly, in the case of position 58, the conservative replacement of lysine by arginine produced an even larger decrease in the affinity of the enzyme for nitrate (i.e., 15-fold) than did replacement by glutamine. In contrast, at position

130, the conservative replacement of lysine by arginine produced a slightly smaller decrease in affinity (i.e., 13-fold), than was the case for replacement by glutamine. In assessing the significance of these K_d values for nitrate binding, it should be mentioned that these values were obtained by studying the spectral perturbations resulting from nitrate binding to the oxidized enzyme. However, it is possible that this process does not play a significant role during the catalytic cycle of the enzyme and, in fact, there is some evidence (5) that nitrate binding during catalysis is more likely to involve a reduced form of the enzyme. A similar situation has been documented in the case of the ferredoxin-dependent spinach chloroplast nitrite reductase, where nitrite binds to form a well-characterized complex with the oxidized enzyme but at a rate that is ca. 10,000 time slower that the known turnover rate of the enzyme and that, in fact, the enzyme must first be reduced by ferredoxin in order for rapid binding of nitrite to occur (28–30).

Discussion

The results presented above, obtained with the *Synechococcus* sp. PCC 7942 enzyme, provide the first evidence that two conserved basic residues, Lys58, and Arg70, are essential for activity in a ferredoxin-dependent cyanobacterial nitrate reductase. The results also support the hypothesis that the requirements at these two positions are specific for lysine at position 58 and for arginine at position 70, as conservative lysine/arginine replacements produce completely inactive enzymes. Evidence has also been obtained for the possibility that a third residue, Lys130, may also play an important role in producing an active enzyme. However, unlike the case at positions 58 and 70, the conservative replacement of the positively charged Lys130 by a positively-charged arginine produces a variant which retains a much larger percentage of the wild-type activity, suggesting that all that is required at this position is the positive charge. A fourth conserved basic residue, Arg146, does not appear to play any role in either substrate binding or catalysis. The observation that replacement of Arg146 by glutamine causes only a negligible loss in activity with either ferredoxin or with MV as the electron donor, in contrast to the very large losses in activity when each of the other three residues are replaced by glutamine, serves as a useful control, eliminating the possibility that the replacement of any conserved basic amino acid in nitrate reductase by glutamine causes a non-specific loss of catalytic function. In the case of Lys58, Arg70 and Lys130, the relatively modest effects on K_M and K_d values for both substrates caused by the replacements by glutamine, compared to those on V_{max}, suggest none of the three conserved amino acids are directly involved in binding either nitrate or ferredoxin.

It might well have been anticipated that replacement of Lys58 by glutamine would have a large effect on activity, considering its likely close proximity to both of the enzyme's prosthetic groups (Table 1) and its likely interactions with the enzyme's MoMGD moiety and with the enzyme's [4Fe-4S] cluster (see, for example, Ref. 11 and 12). Based upon the structural model, Lys58 may be directly involved in controlling electron transfer involving the [4Fe-4S] cluster and Mo center. Arg70 is predicted (Table 1) to make a close approach (i.e., 6.6 Å) to one of the enzyme's two MGD groups in our *in silico* model. However, in the structure of the *D. sulfuricans* nitrate reductase that was used as the basis for the model, Arg62 (the residue that corresponds to Arg70 in the *Synechococcus* sp. PCC 7942 enzyme) does not interact directly with either of the enzyme's two MGD groups (11) and so the rationale for an essential role for Arg70 in the cyanobacterial enzyme remains to be elucidated. It is clear, in the case of Lys130, that proximity to the enzyme's prosthetic groups cannot, in itself, provide an explanation for the observation that it has considerably lower activity than the wild-type enzyme. In the model, Lys130 forms a salt bridge with Glu516 and Arg146 is within hydrogen bonding distance of His358 and Thr391. Thus, the alteration of Lys130 or Arg146 may be compensated by protonation changes in the nearby residues.

The results presented above do not represent the first use of mutagenesis to identify essential amino acids in a ferredoxin-dependent cyanobacterial nitrate reductase. In the initial characterization of the *Synechococcus* sp. PCC 7942 enzyme, mutagenesis was used to investigate the role of Cys9, Cys12, Cys16 and Cys56 as ligands to the four irons in the [4Fe-4S] cluster and of Cys148 as a ligand to Mo (3). Mutagenesis has also been used to provide evidence for a possible role for Arg352 and Met149 (which correspond to Arg351 and Met149, respectively, in *Synechococcus* sp. PCC 7942 nitrate reductase) in nitrate binding by the ferredoxin-dependent nitrate reductase from the cyanobacterium *Cyanothece* sp. PCC 8801 (31). Identification of additional targets for mutagenesis in *Synechococcus* sp. PCC 7942 nitrate reductase will be greatly facilitated by the availability of a three-dimensional structure for the enzyme. To that end, efforts are underway in our laboratories to obtain diffraction-quality crystals of the enzyme and of its complexes with nitrate and with *Synechocystis* sp. PCC 6803 ferredoxin. Until these structures become available, we will use refined versions of the model shown in Figure 2 to guide future mutagenesis studies.

Acknowledgments

Funding

The mutagenesis, protein expression and purification, kinetic measurements and substrate-binding determinations carried out at Texas Tech University were funded by the Division of Chemical Sciences, Geosciences, and Biosciences, Office of Basic Energy Sciences of the U.S. Department of Energy, through Grant DE-FG03-99ER20346 (to D.B.K.). Identification of conserved arginine and lysine residues and contributions to experimental design and data interpretation, carried out at the C.S.I.C. and the Universidad de Sevilla, was funded by grant BFU2008-03811 from the Spanish Government (to E.F.) and was co-financed by a grant from FEDER (to E.F.). Similar contributions, carried out at the Universidad Politécnica de Madrid, were funded by a grant (BIO2009-12661 to L.M.R.) from the Spanish Government. The *in silico* structural modeling and the Fe and Mo determinations, carried out at Arizona State University, was supported by National Science Foundation grant CHE 1158552 (to J.P.A.). Funding for the EPR spectrometry and spin quantitation measurements was provided by the National Institutes of Health, through Grant GM62524 (to M.K.J.).

The authors would like to thank Prof. Clark Lagarias (Department of Molecular and Cellular Biology, University of California, Davis) for the gift of a plasmid encoding the *Synechococcus* sp. PCC 7002 ferredoxin.

Abbreviations

CD	circular dichroism
EPR	electron paramagnetic resonance
Fd	ferredoxin
HEPES	4-(2-hydroxyethyl)-1-piperazineethanesulfonic acid
ICP	inductively-coupled plasma
IPTG	isopropyl-β-D-thiogalactopyranoside
LB	Luria-Bertani
MALDI-TOF	matrix-assisted laser desorption ionization, time-of-flight
MGD	molybdopterin guanine dinucleotide
MV	methyl viologen
NMR	nuclear magnetic resonance
PCR	polymerase chain reaction
PMSF	phenylmethylsulfonyl fluoride

SDS-PAGE	polyacrylamide gel electrophoresis in the presence of sodium dodecylsulfate
UV	ultraviolet

References

1. Flores E, Frías JE, Rubio LM, Herrero A. Photosynthetic nitrate assimilation in cyanobacteria. Photosyn Res. 2005; 83:117–133. [PubMed: 16143847]
2. Hase, T.; Schürmann, P.; Knaff, DB. The interaction of ferredoxin with ferredoxin-dependent enzymes. In: Golbeck, JH., editor. Photosystem 1. Springer; Dordrecht: 2006. p. 477-498.
3. Suzuki A, Knaff DB. Nitrogen metabolism and roles of glutamate synthase in higher plants. Photosyn Res. 2005; 83:191–217. [PubMed: 16143852]
4. Rubio LM, Flores E, Herrero A. Purification, cofactor analysis, and site-directed mutagenesis of *Synechococcus* ferredoxin-nitrate reductase. Photosyn Res. 2002; 72:13–26. [PubMed: 16228531]
5. Jepson BJN, Anderson LJ, Rubio LM, Taylor CJ, Butler CS, Flores E, Herrero A, Burt JN, Richardson DJ. Tuning a nitrate reductase for function. The first spectropotentiometric characterization of a bacterial assimilatory nitrate reductase reveals novel redox properties. J Biol Chem. 2004; 279:322112–32218.
6. Hirasawa M, Rubio LM, Griffin JL, Flores E, Herrero A, Li J, Kim S-K, Hurley JK, Tollin G, Knaff DB. Complex formation between ferredoxin and *Synechococcus* ferredoxin:nitrate oxidoreductase. Biochim Biophys Acta. 2004; 1608:155–162. [PubMed: 14871493]
7. Shih PM, Wu D, Latifi A, Axen SD, Fewer DP, Talla E, Calteau A, Cai F, Tandeau de Marsac N, Rippka R, Herdman M, Sivonen K, Coursin T, Laurent T, Goodwin L, Nolan M, Davenport KW, Han CS, Rubin EM, Eisen JA, Woyke T, Gugger M, Kerfeld CA. Improving the coverage of the cyanobacterial phylum using diversity-driven genome sequencing. Proc US Natl Acad of Sci. 2013; 110:1053–1058.
8. Arnoux P, Sabaty M, Alric J, Frangioni B, Guigliarelli B, Adriano JM, Pignol D. Structural and redox plasticity in the heterodimeric periplasmic nitrate reductase. Nature Struct Biol. 2003; 10:928–934. [PubMed: 14528294]
9. Kisker C, Schindelin H, Rees DC. Molybdenum-cofactor containing enzymes: Structure and mechanism. Annu Rev Biochem. 1997; 66:233–267. [PubMed: 9242907]
10. Romão MJ, Moura JJG, Knäblein J, Huber R. Structure and function of molybdopterin containing enzymes. Prog Biophys Mol Biol. 1997; 68:121–144. [PubMed: 9652170]
11. Dias JM, Than ME, Humm A, Huber R, Bourenkov GP, Bartunik HD, Bursakov S, Calvete J, Caldeira J, Carneiro C, Moura JJG, Moura I, Romão MJ. Crystal structure of the first dissimilatory nitrate reductase at 1.9 Å solved by MAD methods. Structure. 1999; 7:65–79. [PubMed: 10368307]
12. Najmudin S, González PJ, Trincão J, Coelho C, Mukhopadhyay A, Cerqueira NM, Romão FSA, Moura I, Moura JJG, Brondino CD, Romão MJ. Periplasmic nitrate reductase revisited: a sulfur atom completes the sixth coordination of the catalytic molybdenum. J Biol Inorg Chem. 2008; 13:737–753. [PubMed: 18327621]
13. Barth P, Guillouard I, Sétif P, Lagoutte B. Essential role of a single arginine of Photosystem I in stabilizing the electron transfer complex with ferredoxin. J Biol Chem. 2000; 275:7030–7036. [PubMed: 10702267]
14. Tagawa K, Arnon DI. Ferredoxins as electron carriers in photosynthesis and in the biochemical production and consumption of hydrogen gas. Nature. 1962; 195:537–543. [PubMed: 14039612]
15. Aasa R, Vänngård T. EPR signal intensity and powder shapes: A reexamination. J Magn Reson. 2000; 19:308–315.
16. Bradford MM. A rapid and sensitive for the quantitation of microgram quantities of protein utilizing the principle of protein-dye binding. Anal Biochem. 1976; 72:248–254. [PubMed: 942051]

17. Siegel LM, Murphy MJ, Kamin H. Reduced nicotinamide adenine dinucleotidephosphae-sulfite reductase of enterobacteria I. The *Escherichia coli* hemoflavoprotein: Molecular parameters and prosthetic groups. J Biol Chem. 1973; 248:251–264. [PubMed: 4144254]
18. Emsley P, Lohkamp B, Scott WG, Cowlam K. Features and development of *Coot*. Acta Cryts. 2010; D66:486–501.
19. Pettersen EF, Goddard TD, Huang CC, Couch GS, Greenblatt DM, Meng EC, Ferrin TE. UCSF Chimera—A Visualization System for Exploratory Research and Analysis. J Comput Chem. 2004; 25:1605–1612. [PubMed: 15264254]
20. van den Heuvel RH, Svergun DI, Petoukov MV, Curti B, Ravisio S, Vanoni MA, Mattevi A. The active conformation of glutamate synthase and its binding to ferredoxin. J Mol Biol. 2003; 330:113–128. [PubMed: 12818206]
21. Dai S, Friemann R, Glauser DA, Bourquin F, Manieri W, Schürmann P, Eklund H. Structural snapshots along the pathway of ferredoxin-thioredoxin reductase. Nature. 2007; 448:92–96. [PubMed: 17611542]
22. Lelong C, Sétif P, Bottin H, André F, Neumann J-M. ^{1}H and ^{15}N NMR sequential assignment, secondary structure, and tertiary fold of [2Fe-2S] ferredoxin from Synechocystis sp. PCC 6803. Biochemistry. 1005; 34:14462–14473. [PubMed: 7578051]
23. Xu X, Scanu S, Chung J-S, Hirasawa M, Knaff DB, Ubbink M. Structural and functional characterization of the Ga-substituted ferredoxin from Synechocystis sp. PCC6803, a mimic of the native protein. Biochemistry. 2010; 49:7790–7797. [PubMed: 20690702]
24. Hettmann T, Siddiqui RA, von Langen J, Frey C, Romão MJ, Diekmann S. Mutagenesis study on the role of a lysine residue highly conserved in formate dehydrogenases and periplasmic nitrate reductases. Biochem Biophys Res Comm. 2003; 310:40–47. [PubMed: 14511645]
25. Johnson MK, Duderstadt RE, Duin EC. Biological and synthetic $[Fe_3S_4]$ clusters. Adv Inorg Chem. 1999; 47:1–82.
26. González PJ, Rivas MG, Brondino CD, Bursakov SA, Moura I, Moura JJG. EPR and redox properties of periplasmic nitrate reductase from *Desulfovibrio desulfuricans* 27774. J Biol Inorg Chem. 2006; 11:609–616. [PubMed: 16791644]
27. Morales R, Chron M-H, Hudry-Clergeon G, Pétillot Y, Norager S, Medina M, Frey M. Refined X-ray structures of the oxidized, at 1.3 Å, and reduced, at 1.17 Å, [2Fe-2S] ferredoxin from the cyanobacterium *Anabaena* PCC7119 show redox-linked conformational changes. Biochemistry. 1999; 38:15764–15773. [PubMed: 10625442]
28. Kuznetsova S, Knaff DB, Hirasawa M, Lagoutte B, Sétif P. Mechanism of spinach chloroplast ferredoxin-dependent nitrite reductase: Spectroscopic evidence for intermediate states. Biochemistry. 2004; 43:510–517. [PubMed: 14717606]
29. Kuznetsova S, Knaff DB, Hirasawa M, Sétif P, Mattioli TA. Reactions of spinach nitrite reductase with its substrate, nitrite, and a putative intermediate, hydroxylamine. Biochemistry. 2004; 44:10765–10774. [PubMed: 15311938]
30. Sétif P, Hirasawa M, Cassan N, Lagoutte B, Tripathy JN, Knaff DB. New insights into the catalytic cycle of plant nitrite reductase. Electron transfer kinetics and charge storage. Biochemistry. 2009; 48:2828–2838. [PubMed: 19226104]
31. Wang TH, Chen YH, Huang JY, Liu KC, Ke SC, Chu HA. Enzyme kinetics, inhibitors, mutagenesis and electron paramagnetic resonance analysis of dual-affinity nitrate reductase in unicellular N_2-fixing cyanobacterium *Cyanothece* sp. PCC 8801. Plant Physiol and Biochem. 2011; 49:1369–1376. [PubMed: 21821424]

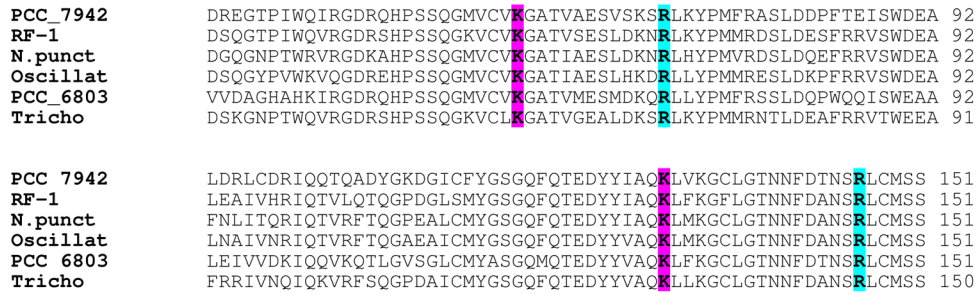

Figure 1.

An amino acid sequence alignment of six ferredoxin-depenedent cyanobacterial nitrate reductases. The N-terminal and C-terminal regions of the enzymes have not been included. The species listed are: **PCC 7942,** *Synechococcus* sp. PCC 7942; **RF-1,** *Synechococcus* RF-1; **N. punct,** *Nostoc punctiforme*, **Oscillat,** *Oscillatoria*; **PCC 6803,** *Synechocystis* sp. PCC 6803; and **Tricho,** Trichodesmium. Lysines 58 and 130 in *Synechococcus* sp. PCC 7942 nitrate reductase, and the corresponding lysines in the nitrate reductases from the five other species, are highlighted in magenta. Arginines 70 and 146 in *Synechococcus* sp. PCC 7942 nitrate reductase, and the corresponding arginines in the nitrate reductases from the five other species, are highlighted in turquoise.

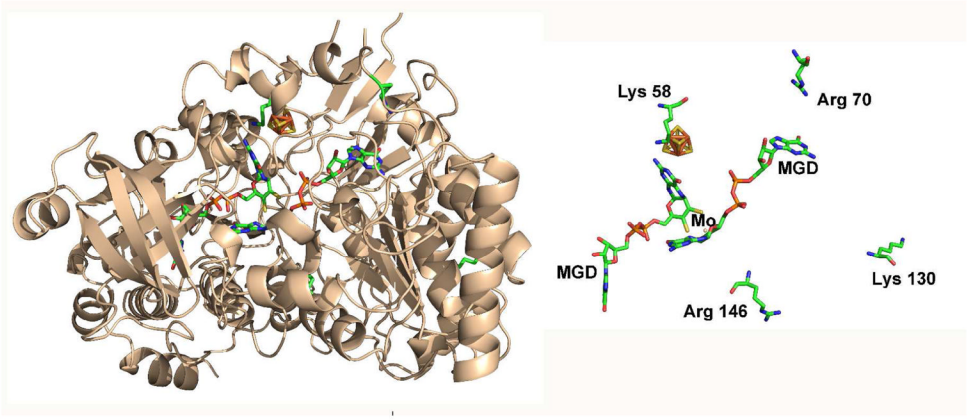

Figure 2.

An *in silico* model for the structure of *Synechococcus* sp. PCC *7942* nitrate reductase showing the full model (left) and the cofactors and selected residues (right). The four residues targeted for mutagenesis are identified by their amino acid sequence numbers. The four side chains and cofactors are colored according to atom type. The right-hand figure is rotated by 90° about the x axis relative to the left-hand figure.

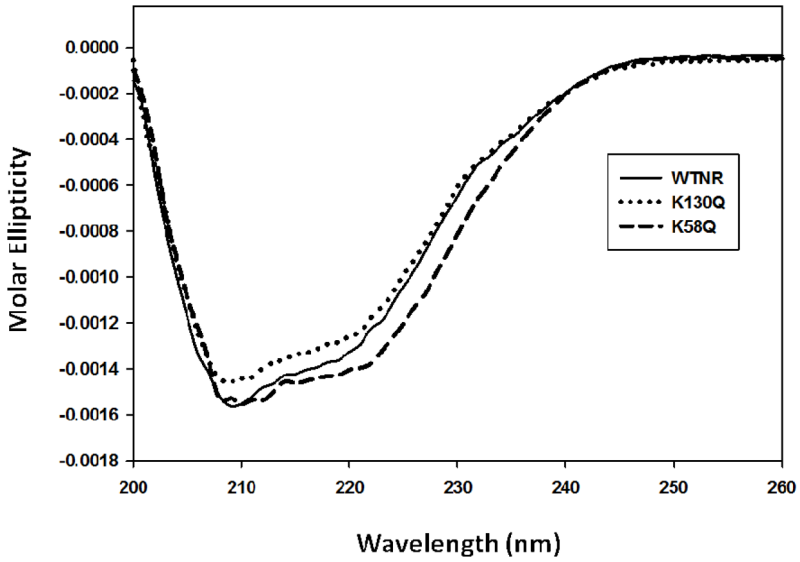

Figure 3.

Circular dichroism spectra of wild-type nitrate reductase and its K58Q and K130Q variants. Spectra were measured at ambient temperature in a 1.0 cm optical pathlength cell using solutions of either wild-type nitrate reductase or the indicated variant. All samples contained nitrate reductase at a concentration of 0.75 μM in 10 mM potassium phosphate buffer (pH 7.5).

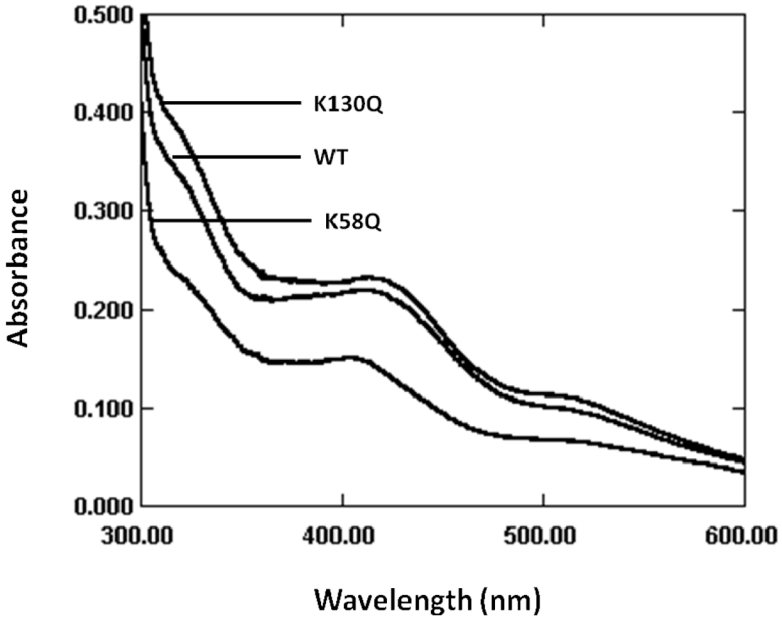

Figure 4.

UV/visible absorbance spectra of wild-type nitrate reductase and its K58Q and K130Q variants. Spectra were measured at ambient temperature in a 1.0 cm optical pathlength cell using solutions of either wild-type nitrate reductase or the indicated variant. All samples contained nitrate reductase at a concentration of 15 μM in 25 mM HEPES buffer (pH 8.0).

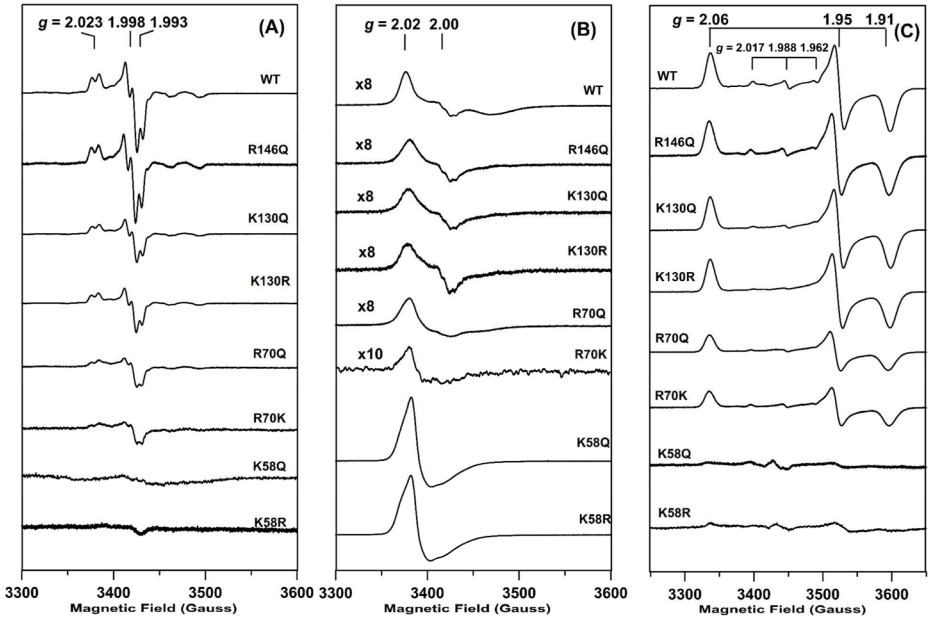

Figure 5.

EPR spectra of wild-type nitrate reductase and the R146Q, K130Q, K130R, R70Q, R70K, K58Q, and K58R variants. (A) Air-oxidized samples recorded at 70 K and 2 mW microwave power. (B) Air-oxidized samples recorded at 10 K and 1 mW microwave power. (C) Dithionite-reduced samples recorded at 20 K and 1 mW. Protein concentrations in the samples ranged from 0.3 to 0.7 mM and the buffering medium was 25 mM HEPES with 200 mM NaCl and 100 μM sodium molybdate. All spectra were recorded at 9.60 GHz and 6.0 Gauss modulation amplitude and the intensities have been normalized to correct for differences in spectrometer gain and sample protein concentration.

Table 1

Distances between the four residues targeted for mutagenic replacement and the prosthetic groups of nitrate reductase.

Residue	Distance to Fe/S cluster* (Å)	Distance to Proximal MGD moiety* (Å)	Distance to Distal MGD moiety* (Å)
Lys 58	4.3	3.0	19.8
Arg 70	17.6	19.3	6.6
Lys 130	30.7	30.2	22.0
Arg 146	24.6	14.8	20.9

* Distances are measured from the end of each side chain to the closest point of each cofactor.

Table 2

Primers used to introduce mutation in the pCSLM85 nitrate reductase expression plasmid.

Primer Name	Sequence (5′-3′)
K58Q-For	GGAATGGTCTGCGTC**CAG**GGCGCAACGGTGGCG
K58Q-Rev	CGCCACCGTTGCGCC**CTG**GACGCAGACCATTCC
K58R-For	GGAATGGTCTGCGTC**AGA**GGCGCAACGGTGGCG
K58R-Rev	CGCCACCGTTGCGCC**TCT**GACGCAGACCATTCC
R70Q-For	TCTGTCAGCAAAAGC**CAG**CTGAAATATCCAATG
R70Q-Rev	CATTGGATATTTCAG**CTG**GCTTTTGCTGACAGA
R70K-For	TCTGTCAGCAAAAGC**AAG**CTGAAATATCCAATG
R70K-Rev	CATTGGATATTTCAG**CTT**GCTTTTGCTGACAGA
K130Q-For	TACTACATCGCCCAA**CAG**CTGGTGAAAGGTTGC
K130Q-Rev	GCAACCTTTCACCAG**CTG**TTGGGCGATGTAGTA
K130R-For	TACTACATCGCCCAA**CGG**CTGGTGAAAGGTTGC
K130R-Rev	GCAACCTTTCACCAG**CCG**TTGGGCGATGTAGTA
K146Q-For	TTCGATACCAACTCG**CAG**CTCTGCATGTCCTCA
K146Q-Rev	TGAGCACATGCAGAG**CTG**CGAGTTGGTATCGAA

Table 3

Kinetic properties of wild-type nitrate reductase and four variants

Enzyme	Fd K_M (μM)	NO_3^- K_M (μM)	Relative MV-linked specific activity[a]	Relative Fd-linked specific activity[b]
Wild-Type	38.0±3.7	6.0±1.0	100	100
K58Q	nd	Nd	<0.1	<0.1
K58R	nd	Nd	<0.1	<0.1
R70Q	nd	nd	<0.1	<0.1
R70K	nd	nd	<0.1	<0.1
K130Q	106±17	3.3±0.5	26	22
K130R	40.0±8.0	5.7±2.5	55	65
R146Q	51.0±5.0	2.5±0.3	91	87

[a] 100% = 860 μmol of nitrite produced/min/mg enzyme

[b] 100%= 35.0±2.2 μmol of nitrite produced/min/mg enzyme

nd = Not determined

Table 4

Prosthetic group content and substrate-binding affinities of wild type nitrate reductase and its variants.

Enzyme	Sulfide[a]	Iron[a]	Molybdenum[a]	K_d Nitrate (μM)	K_d Ferredoxin (μM)
Wild Type	3.5±0.2	3.5±0.77	0.80±0.34	1.0±0.3	7.8±2.1
K58Q	2.7±0.18	0.7±0.18	0.80±0.15	8.0±2.3	85.0±9.6
K58R	2.8±0.22	1.1±0.31	0.19±0.08	15.5±5.0	7.5±2.6
R70Q	2.8±0.16	2.1±0.57	0.67±0.27	5.5±2.2	3.0±1.0
R70K	3.0±0.29	1.6±0.12	0.36±0.08	6.0±1.0	3.2±1.7
K130Q	3.1±0.24	3.6±0.15	0.39±0.02	19.0±6.8	12.6±2.4
K130R	3.4±0.28	3.0±0.075	0.46±0.02	13.4±3.0	8.0±0.2
R146Q	3.2±0.31	3.8±0.44	1.07±0.11	1.5±0.4	2.6±0.3

[a] mol/mol of enzyme